

# Passage of millicharged particles in the electron beam-dump: refining constraints from SLACmQ and estimating sensitivity of NA64e.

Nataliya Arefyeva,<sup>1,2</sup> Sergei Gninenko,<sup>2</sup> Dmitry Gorbunov,<sup>2,3</sup> and Dmitry Kirpichnikov<sup>2</sup>

<sup>1</sup>*Physical Department, Lomonosov Moscow State University, Vorobiovy Gory, Moscow 119991, Russia*

<sup>2</sup>*Institute for Nuclear Research of the Russian Academy of Sciences, 117312 Moscow, Russia*

<sup>3</sup>*Moscow Institute of Physics and Technology, Institutsky lane 9, Dolgoprudny, Moscow region, 141700, Russia*

(Dated: April 22, 2022)

Millicharged particles (MCPs) arise in many well-motivated extensions of the Standard Model and are a popular subject for experimental searches. We investigate attenuation of the MCP flux produced at accelerator experiments due to their interactions in the media. Considering, as an example, the dedicated MCP search at SLACmQ, we demonstrate that this effect can significantly affect the final sensitivity to the MCP parameter space leaving its essential part still unexplored. Applying our analysis to the SLACmQ experiment [53], we correct their exclusion bounds in close accordance with Ref. [54]. We also show that this newly reopened area with the MCP masses in the range  $10^{-4}$  eV - 1 GeV and charges  $\gtrsim 10^{-5}e$  can be effectively probed by the NA64e experiment at the CERN SPS. Light MCPs are mostly produced by virtual photon in electron scattering off nucleus. The main source of heavy MCP is decays of vector mesons, produced by the electrons on nuclei.

## I. INTRODUCTION

The millicharged particles (MCPs) are considered in connection with electric charge quantization mechanism and new physics models with electric charge non-conservation [1]. Moreover, scenarios beyond the Standard Model (SM) of particle physics can naturally include particles, which electric charge is a small fraction of the electron charge,  $Q_\chi = e\epsilon \ll e$ . In particular, the millicharged particles can be considered as a well-motivated dark-matter candidate [2–8]. Thus, experimental searches for such particles are of a great interest [9].

The simplest way to introduce the MCPs in a model is to consider them as a low-energy limit of the theory, where a hidden (dark) photon,  $A'_\mu$ , kinetically mixes with the visible SM photon  $A_\mu$  [10]. As a result, e.g. a new fermion of the hidden sector  $\chi$ , coupled to the hidden photon, can acquire a small electric charge  $\sim e\epsilon$ , and the model Lagrangian can be written as follows

$$\mathcal{L} \supset i\bar{\chi}\gamma^\mu\partial_\mu\chi - m_\chi\bar{\chi}\chi + e\epsilon A_\mu\bar{\chi}\gamma^\mu\chi, \quad (1)$$

where  $m_\chi$  is the Dirac mass of the hidden MCP.

The parameter space of the MCP on  $(\epsilon, m_\chi)$  plane can be constrained from the searches at collider [11–19] and fixed-target [20–28] experiments, with optical sensors [29–31] and searches with a superconducting radio-frequency cavity [32], from analysis of cosmological and astrophysical observations [33–45], and by using results of cosmic-ray detectors [46–48] and nuclear reactor experiments [49–51], etc.

In accelerator experiments, the MCPs can be produced at intense proton fixed-target facilities in decays of mesons

$$\pi^0, \eta, \eta' \rightarrow \gamma\chi\bar{\chi}, \quad \rho, \omega, \phi, J/\psi \rightarrow \chi\bar{\chi}, \quad (2)$$

from hadronic showers initiated by high-energy protons in a dump. A thick shield between the production and

detection points of the MCP absorbs all strongly and electromagnetically interacting secondary particles, while the MCP may pass through the shield and can be detected in a far detector via their scattering off electrons,  $\chi e^- \rightarrow \chi e^-$ . In this case the observation of MCP is based on a search for excess of low-energy recoil electrons in the detector. The number of signal events  $N_\chi$  in such type of experiments, scales as  $N_\chi \propto \epsilon^4$  for a single MCP hit in the detector, and as  $N_\chi \propto \epsilon^6$  for the double-hit MCP signature [23]. Consequently, a large number of protons on target, POT, is required to probe small values of  $\epsilon$ . E.g., for, say,  $\epsilon \lesssim 10^{-3}$  and MCP masses  $m_\chi \gtrsim 100$  MeV, one needs  $\sim \mathcal{O}(10^{20}) - \mathcal{O}(10^{22})$  POT.

A more powerful and effective approach in probing MCP can be based on their production in high energy electrons scattering off heavy nuclei, the process exploited by the NA64e experiment in the North Area of the CERN SPS. The NA64e facility has been originally designed for searching for Light Dark Matter (LDM) production in invisible decays of a dark photon ( $A'$ ) mediator in the reaction chain,  $e^-N \rightarrow e^-NA'; A' \rightarrow \text{LDM}$  [52]. That approach can be also adopted for searching for MCP in missing energy events due to the MCP production in the reaction  $eN \rightarrow e^-N\gamma^* \rightarrow e^-N\chi\bar{\chi}$  accompanied by missing energy carried away by the MCP pair. The expected number of signal events in this case is proportional to  $N_\chi \propto \epsilon^2$ . Therefore, a much lower number of electrons on target (EOT),  $n_{EOT} \simeq \mathcal{O}(10^{12}) - \mathcal{O}(10^{13})$  is required to test the same region of at small values  $\epsilon \lesssim 10^{-3}$  [52] as compared to the required number of POT.

Another point, discussed in this work, is related to the attenuation of a charged particle flux while propagating in matter. The energy losses and multiple scattering of charged particles strongly depend on the their charge to mass ratio, as we well know from the comparison of the electron and muon propagation in media. Therefore, for the relatively light MCP in the mass range,  $m_\chi \lesssim 10$  MeV, and a small charge  $\epsilon \lesssim 10^{-5} - 10^{-1}$ , the

search sensitivity of beam-dump experiments, such, e.g. as SLACmQ [53], might be constrained by a significant attenuation of the MCP flux at the detector location.

In this paper we reconsider part of the MCP bounds from the SLACmQ beam-dump experiment taking into account the MCP flux attenuation due to i) MCP energy loss in the reactions of  $\chi e^- \rightarrow \chi e^-$  scattering, pair production,  $\chi N \rightarrow \chi N e^+ e^-$ , bremsstrahlung,  $\chi N \rightarrow \chi N \gamma$  and ii) decreasing of the MCP deflection acceptance due to the MCP multiple scattering in the dump. We show that indeed, altogether these processes may prevent the MCP from reaching the SLAC mQ detector and giving the signal. We find that our revised results on MCP sensitivity are in a fairly good agreement with previous study [54]. We implement the developed ideas of MCP stopping power calculation for the estimate of expected reach of NA64e in the region of model parameter space,  $m_\chi \lesssim 100$  MeV and  $\epsilon \lesssim 10^{-5} - 10^{-1}$ . We also calculate and find it promising, the expected sensitivity of NA64e to MCP, produced in bremsstrahlung-like events,  $eN \rightarrow eN \gamma^* (\rightarrow \chi \bar{\chi})$  and to MCP, emerged in invisible decays of short-lived vector mesons  $V = \{\rho, \omega, \phi, J/\psi\}$ , produced in the reaction of photo-production inside the dump,  $\gamma^* N \rightarrow NV (\rightarrow \chi \bar{\chi})$  for  $m_\chi \gtrsim 10$  MeV and  $10^{-3} \lesssim \epsilon \lesssim 10^{-2}$ .

The paper is structured as follows. Section II describes various effects associated with MCP passage through matter, namely: the dominant MCP energy losses in matter (ionization and radiation losses via bremsstrahlung and  $e^+e^-$  pair production) and the deflection of MCP trajectory due to multiple scattering. In Section III we implement the results of Section II to revise the analysis of the SLACmQ experiment [53] and correct their exclusion region in  $(m_\chi, \epsilon)$  parameter space. In Section IV we calculate the exact tree-level cross section of the process  $eN \rightarrow eN \gamma^* (\rightarrow \chi \bar{\chi})$  to estimate the yield of the MCP in the NA64e missing energy signature. In Section V we estimate the NA64e prospects in probing MCP models for the relatively wide mass range  $10^{-4}$  eV  $\lesssim m_\chi \lesssim 1$  GeV. In Section VI we estimate the expected reach of NA64e to examine MCPs from invisible decay of vector mesons. We conclude in Section VII. Two appendices contain some formulas used in the numerical calculations.

## II. MCP INTERACTIONS IN MATTER

High energy particles can produce sufficiently light MCPs by scattering off target. In turn, the MCP collides with electrons and nuclei of the dump material resulting in energy losses and multiple scattering, and thus, deviation from its original direction, when passing through matter. In this Section we consider three processes of MCP energy losses: ionization, radiation and pair production, some of which are illustrated with Fig. 1. In the end of Section we estimate a typical angle of MCP deviation from the original direction due to the multiple

scattering.

### A. Ionization losses

Ionization energy losses are associated with the MCP collision with an atom, which initiates the atom excitation and knocking out the electron, see Fig. 1(a1). To quantify the ionization losses effect for MCP we adopt the Bethe–Bloch formula as [55]:

$$\left(-\frac{dE_\chi}{dx}\right)_{\text{ion}} = \frac{4\pi Z \epsilon^2 r_e^2 m_e}{\beta_\chi^2} \frac{N_A \rho}{M_A} \times \left(\frac{1}{2} \ln \frac{2m_e \beta_\chi^2 \gamma_\chi^2 T_{max}}{I^2} - \beta_\chi^2 - \frac{\delta(\beta_\chi \gamma_\chi)}{2}\right) \quad (3)$$

where  $x$  is the track length of MCP,  $\beta_\chi$  is its velocity and  $\gamma_\chi = E_\chi/m_\chi$  is its Lorentz factor. The last term in (3) comes from the matter polarization, and at very high energies,  $\gamma_\chi \gg 1$ , it approaches  $\delta(\beta_\chi \gamma_\chi) \approx 2 \log(\omega_p \beta_\chi \gamma_\chi / I) - 1$ . Then  $I$  stands for the ionization potential of the atom,  $r_e = \alpha/m_e \simeq 2.8$  fm is the classical radius of electron,  $N_A = 6.02 \cdot 10^{23} \text{ mol}^{-1}$  is the Avogadro's number,  $Z$  is the atomic number of target material,  $M_A$  is the atomic mass of the target material and  $\rho$  is its density, the maximum energy transferred from MCP to electron is given by

$$T_{max} = \frac{2m_e \beta_\chi^2 \gamma_\chi^2}{1 + 2\gamma_\chi m_e/m_\chi + m_e^2/m_\chi^2}. \quad (4)$$

We note, that the MCP's ionization stopping power (3) scales as  $\propto \epsilon^2$  and depends logarithmic on  $E_\chi$  and  $m_\chi$  in the ultra-relativistic regime  $\beta_\chi \simeq 1$ .

### B. Radiation losses

The MCP slow down due to scattering off nuclei in the material and emission of photons as illustrated by the Feynman diagrams in Fig. 1(b). The radiation loss due to scattering off electrons is suppressed by the nuclear charge as  $1/Z$ , and we neglect it in our study.

The atomic electrons outside the nucleus screen the nucleus Coulomb field, so that its effective strength decreases and atomic electrons also serve as scattering targets. In our case of ultra relativistic MCP the screening can be considered as a complete one. The MCP energy losses for radiation per unit length is determined by

$$\left(-\frac{dE_\chi}{dx}\right)_{\text{brems}} = n \int_0^{E_\chi - m_\chi} dE_\gamma \frac{d\sigma_{\text{brems}}}{dE_\gamma} E_\gamma, \quad (5)$$

where  $n = N_A \rho / M_A$  is the number density of atoms in the target,  $d\sigma_{\text{brems}}/dE_\gamma$  is the differential bremsstrahlung cross section,  $E_\gamma$  is the energy of the

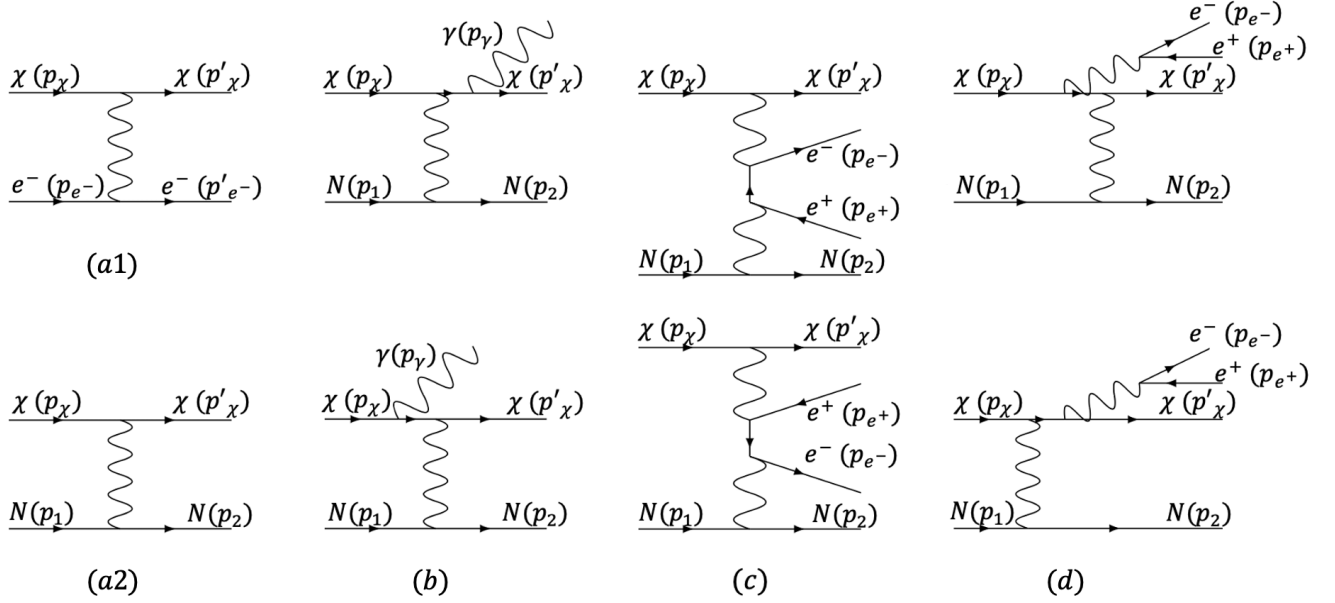


FIG. 1. Feynman diagrams for MCP energy loss in matter: (a) scattering off atomic nucleus and electrons, (b) bremsstrahlung, (c,d)  $e^+e^-$  pair production.

emitted photon. The bremsstrahlung spectrum in the case of complete screening is given by the formula [55]

$$\frac{d\sigma_{\text{brems}}}{dE_\gamma} \simeq \frac{1}{E_\gamma} 4\alpha Z^2 r_e^2 \epsilon^4 \left(\frac{m_e}{m_\chi}\right)^2 \left(\frac{4}{3} - \frac{4E_\gamma}{3E_\chi} + \frac{E_\gamma^2}{E_\chi^2}\right) F_{\text{corr}}, \quad (6)$$

where  $F_{\text{corr}}$  is the factor which takes into account the Coulomb correction to the Born cross section and atomic screening effects [55]. We note that the stopping loss of the MCP due to the radiation scales as  $\propto \epsilon^4 E_\chi/m_\chi^2$ , therefore, the lighter MCPs lose their energy more rapidly.

### C. Electron-positron pair production

MCP energy losses can be accounted by considering the process illustrated with Fig. 1 (c), (d). One observes, that for sufficiently small parameter  $\epsilon$ , the amplitude of Fig. 1 (d) is suppressed due to additional factor  $\epsilon$ . The MCP's energy losses due to the  $e^+e^-$  pair production can be written as

$$\left(-\frac{dE_\chi}{dx}\right)_{e^+e^- \text{ pair}} = n \int_{2m_e}^{E_\chi - m_\chi} d\omega \frac{d\sigma_{e^+e^- \text{ pair}}}{d\omega} \omega, \quad (7)$$

where  $\omega = E_{e^+} + E_{e^-}$  is the total energy of  $e^+e^-$  pair. The cross section  $d\sigma_{e^+e^-}/d\omega$  can be taken [56] in the ultra-relativistic approximation, when the energies of initial and final MCPs are high,  $E'_\chi, E_\chi \gg m_\chi, m_e$ , as well

as the energies of electron and positron,  $E_{e^+}, E_{e^-} \gg m_e$ . In particular, the integration over the energy of positron yields the spectrum of the produced pair,

$$\frac{d\sigma_{e^+e^- \text{ pair}}}{d\omega} = \int_{m_e}^{\omega - m_e} \frac{d\sigma_{e^+e^- \text{ pair}}}{dE_{e^+} dE_{e^-}} dE_{e^+},$$

where the double differential cross section is written as

$$\frac{d\sigma_{e^+e^- \text{ pair}}}{dE_{e^+} dE_{e^-}} = Z^2 \epsilon^2 \frac{\alpha^2 r_e^2}{2\pi} \frac{E'_\chi - \omega}{\omega^2 E_\chi} G, \quad (8)$$

and the value of  $G$  is given in Appendix A.

In the given material the energy losses of all the types depend on the MCP energy  $E_\chi$ , mass  $m_\chi$  and parameter  $\epsilon$ . We illustrate their impacts with plots of Fig. 2. We observe that in different parts of the model parameter space different mechanisms dominate at a given energy. In particular, one can neglect the ionization energy loss of the MCP at energies  $E_\chi \gtrsim 10$  GeV.

The energy loss of the MCP on its way from the production point through the media to the detector, can significantly reduce its energy. It should be taken into account when estimating the energy release in the detector due to the MCP elastic scattering inside the detector, which provides the MCP signal signature. In case of large energy loss the MCP energy may drop below the threshold accepted for the energy release to be observable. Such a low-energy MCP avoids the detection.

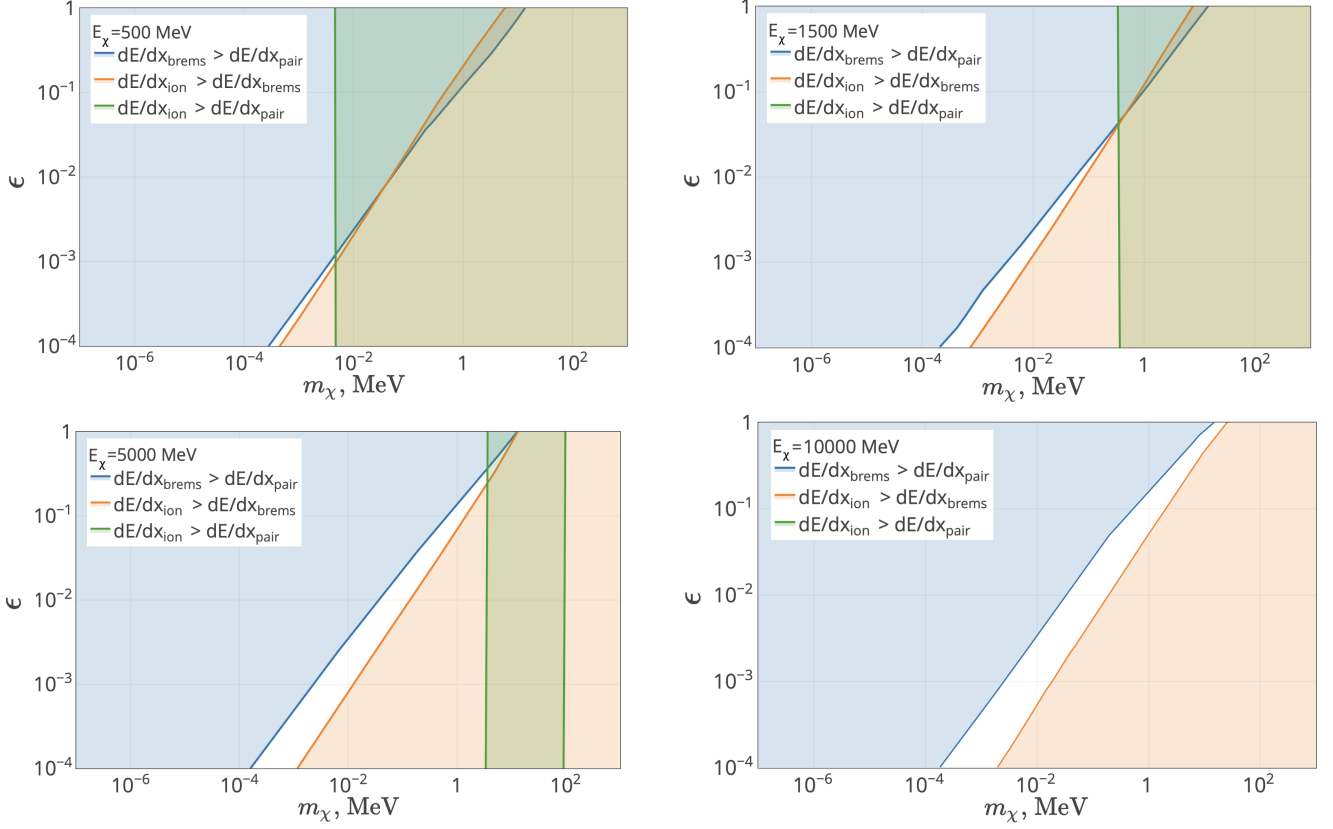


FIG. 2. The diagrams showing in which parts of the model parameter space, which mechanism of the energy loss dominates. There are four plots for MCP energies  $E_\chi = 500$  MeV,  $E_\chi = 1.5$  GeV,  $E_\chi = 5$  GeV,  $E_\chi = 10$  GeV.

#### D. Multiple scattering

We should also take into account the deflection of the MCP trajectory from the rectilinear one, which happens mostly due to multiple elastic scatterings off nuclei and electrons in the media, see the corresponding Feynman diagrams in Fig. 1 (a1) and (a2). For the nucleus case the averaged squared deflection angle of the MCP per unit propagation length reads

$$\frac{d\theta_{\chi Z}^2}{dx} = n \int_0^\pi d\theta_\chi \theta_\chi^2 \frac{d\sigma_{\chi Z}}{d\theta_\chi} \quad (9)$$

with the scattering cross section on a nucleus

$$\frac{d\sigma_{\chi Z}}{d\theta_\chi} = \frac{Z^2 \epsilon^2 r_e^2 m_e^2}{4 E_\chi^2 \beta_\chi^2} \frac{1 - \beta_\chi^2 \sin^2\left(\frac{\theta_\chi}{2}\right)}{\sin^2\left(\frac{\theta_\chi}{2}\right) + 1/(2a p_\chi)^2} 2\pi \sin\theta_\chi, \quad (10)$$

where  $a \simeq 111Z^{-1/3}/m_e$  is the screening parameter for the Thomas–Fermi atoms.

Similarly, for the case of MCP deflection by the atomic electron one has the following expression for the average

squared angle per unit propagation length

$$\frac{d\theta_{\chi e}^2}{dx} = Z \frac{N_A \rho}{M_A} \int_0^\pi \theta_\chi^2 \frac{d\sigma_{\chi e}}{d\theta_\chi} d\theta_\chi \Theta(E_\chi - E'_\chi - \alpha^2 m_e/2), \quad (11)$$

where the differential cross section in the laboratory frame is

$$\frac{d\sigma_{\chi e}}{d\theta_\chi} = \frac{2}{\pi} \sin\theta_\chi \frac{\epsilon^2 r_e^2 m_e |\vec{p}'_\chi|}{E'_e |\vec{p}_\chi|} \times \frac{m_e^2 (E_\chi^2 + E_\chi'^2) + \frac{1}{2}(m_e^2 + m_\chi^2)(2m_\chi^2 - 2(p_\chi p_{\chi'}))}{(2m_\chi^2 - 2(p_\chi p_{\chi'}))^2}. \quad (12)$$

The last term in Eq. (11) is the step-function, which accounts for screening effects. In particular, the additional condition should be imposed on the MCP transfer momentum squared,  $-t = -(p'_\chi - p_\chi)^2 \gtrsim 1/R_{scr}^2$ , where  $R_{scr} \simeq (\alpha m_e)^{-1}$  is the typical screening radius for the atomic electrons. The latter condition implies the following inequality  $E'_\chi \lesssim E_\chi - \frac{\alpha^2}{2} m_e$ , which defines the step-function  $\Theta(x)$  in the integral of (11). It refers to the fact that the energy of the initial electron is below its mass because of the binding energy  $-\alpha^2 m_e/2$ .

### III. REVISITING SLACMQ BOUNDS ON MCPS

In this Section we revise the SLACmQ bounds on MCPs using detailed information on the expected MCP spectra and geometry of the SLACmQ experiment provided in Ref. [54]. In particular, we reconsider the limits associated with MCP stopping power, time resolution and angular acceptance of the SLAC detector. The revised constraints we obtain in this way are similar to the ones from Ref. [54].

#### A. Stopping power

Let us consider first the impact of stopping power on bounds on MCP parameter space obtained by the SLACmQ experiment, see its layout in Fig.3. The SLACmQ collected data of  $3.8 \times 10^{18}$  EOT. It employed a pulsed beam of 29.5 GeV electrons hitting the target made mostly of rhenium (25%) and tungsten (75%). On the way to detector, placed at the distance  $S = 110.1$  m from the target, MCPs passed downstream through sandstone, with effective density  $\rho = 2.19$  g/cm<sup>3</sup> and a length of  $L \simeq 88.5$  m. Note that MCPs are produced in the target mainly due to the bremsstrahlung process,  $eN \rightarrow eN\chi\bar{\chi}$ , which implies that the production cross section scales as  $\propto \alpha^4 \epsilon^2 Z^2$ . Therefore, the number of produced MCP pairs is proportional to  $N_{prod} \propto \epsilon^2$ .

The predominant signature of the MCP used for detection is its elastic scattering off electrons in the far detector,  $\chi e^- \rightarrow \chi e^-$ , see the corresponding diagrams in Fig.1(a1). Hence, assuming  $\epsilon \ll 1$  and MCP reaching the detector, the part of MCPs which hit the electrons on the way through the detector scales as  $N_{det} \propto \epsilon^2$ . In addition, we note that for  $\epsilon \ll 1$  and  $m_\chi \gg m_e$  both the rate of MCP production and their attenuation rate are small. Therefore, as long as the attenuation rate of MCP is negligible the number of expected signal events scales as  $N_{sig} \propto \epsilon^4$ . To set the constraints at a given confidence level (typically 90%C.L. or 95%C.L.) in that region of MCP's parameter space one should set  $s_{up} \simeq N_{sig}$ , where  $s_{up}$  is the upper limit on the average number of signal events for the given sum of signal and background events. In Fig. 6 these bounds correspond to the lower edge of the SLACmQ [54] excluded contour. We adopt that curve from Fig. 5.17 of Ref. [54]. It differs noticeably from the curve presented in the seminal work [53] as the upper limits of SLACmQ on the parameter  $\epsilon$ .

Let us consider the attenuation of the MCP initial energy flow  $I_0$

$$I = I_0 \exp\left(-\frac{L}{X_\chi}\right),$$

where  $X_\chi$  is the MCP attenuation length,  $L$  is the distance traveled by the MCP in matter. In case of the SLACmQ experiment the MCP attenuation length can

be estimated as follows

$$X_\chi = \int_{E_{min}}^{E_{max}} dE_\chi \frac{1}{N} \frac{dN}{dE_\chi} \int_{E_{cut}^\chi}^{E_\chi} \frac{dE'_\chi}{|dE'_\chi/dx|}, \quad (13)$$

where  $E_\chi$  is initial energy of MCP and  $E_{cut}^\chi$  is the energy threshold of MCP detection in the experiment,  $E_{min}=0.125$  GeV, and  $E_{max}=29.5$  GeV is the beam energy [54]. The total energy losses are:

$$\left(\frac{dE_\chi}{dx}\right)_{tot} = \left(\frac{dE_\chi}{dx}\right)_{ion} + \left(\frac{dE_\chi}{dx}\right)_{rad} + \left(\frac{dE_\chi}{dx}\right)_{pair}, \quad (14)$$

the normalized to unity spectra  $N^{-1}dN/dE_\chi$  of the produced MCP are taken from Table A.2 in Appendix of [54], in Fig. 4 we show them for various masses  $m_\chi$ .

The account of attenuation of the MCP passing through the matter changes the upper bound on  $\epsilon$  at a given mass  $m_\chi$  as follows

$$\epsilon^4 = \epsilon_{u.b.}^4 \exp\left(-\frac{L}{X_\chi(\epsilon_{u.b.})}\right), \quad (15)$$

where  $\epsilon$  is the charge value of the MCPs that would reach the detector without energy loss (so that  $s_{up} \propto \epsilon^4$ ), and  $\epsilon_{u.b.}$  is the maximum charge value of the MCP that reach the detector with the proper accounting of their energy losses.

We note that for the relatively large charge,  $\epsilon \gtrsim 10^{-2} - 10^{-1}$ , and  $m_\chi \gtrsim m_e$  the rate of MCP production is fairly high. On the other hand, the rate of MCP absorption in the dump due to ionization and  $e^+e^-$  pair production is also high. Thus, the number of produced MCP is compensated by their attenuation in the dump. Moreover, numerical calculations reveal that for  $\epsilon \ll 1$  and  $m_\chi \lesssim m_e$  the radiation stopping power of MCP is not negligible and plays the dominant role in their absorption in the dump. In Fig. 5 the typical stopping power and its impact on the limit is illustrated for  $X_\chi \simeq L$  and two values of MCP energy at production, which are relevant for SLACmQ experiment.

#### B. Angular and timing acceptance

There are also two important benchmark conditions that should be taken into account to constrain the charge-mass parameter space of MCP in the case of SLACmQ. The first one is associated with the time interval of data taking. The arrival time of the MCPs in the detector is defined by the muon beam scintillating counters located between the target and the detector at the distance of  $S_\mu = 82.6$  m from the target ( $L_\mu = 61$  m through sandstone) as shown in Fig.3. The data are collected during the time interval  $\Delta t_{coll} = 250$  ns. The offset of synchronized signal is such that the muon signals came to muon counters in  $\Delta t_{off} = 60$  ns after the start of main timing window. It is assumed that the muons are (ultra)relativistic and collisionless, hence they reach

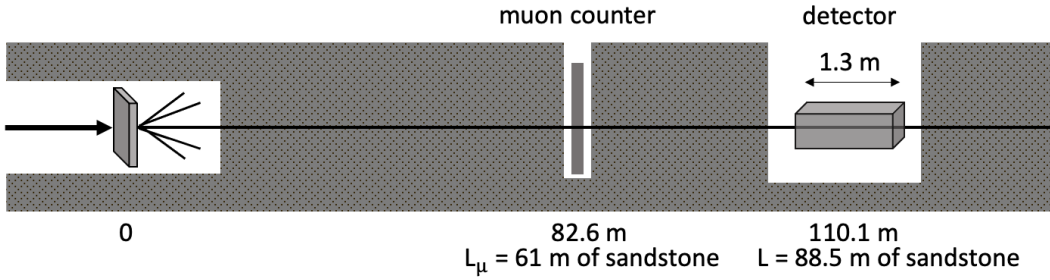


FIG. 3. Layout of SLACmQ experiment.

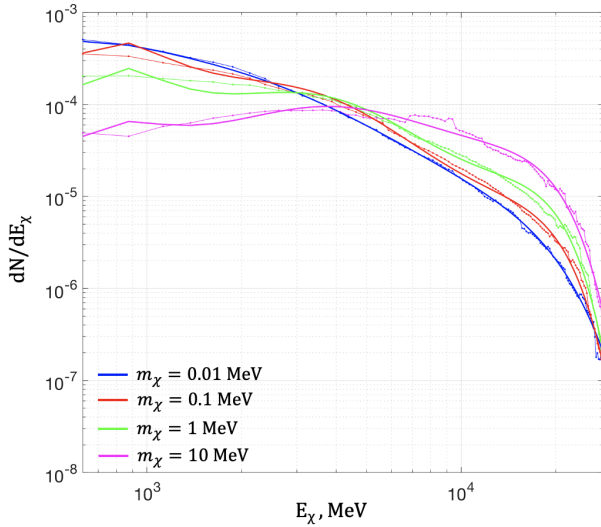


FIG. 4. Approximations to the differential energy spectra from SLACmQ data [54] normalized to unity for a set of MCP masses  $m_\chi$  and  $\epsilon = 10^{-3}$ .

the muon counter without any delay with respect to the light. Indeed, the typical radiation length of the muon can be estimated as  $X_0^\mu \simeq X_0^e (m_\mu/m_e)^2 \simeq 4.4 \cdot 10^4 X_0^e$ , for  $X_0^e \simeq \mathcal{O}(1)$  cm that implies  $X_0^\mu \simeq 440$  m, so that muon loses a small amount of the initial energy when it reaches the detector at the typical distance of 110 m. On the other hand, the produced in the target MCP of energy  $E_i$  can scatter off the sand and reach the muon counter with time delay of

$$\Delta\tau_\mu = \int_{S_\mu}^0 dx \frac{1-\beta}{\beta} = \int_{E_i}^{E_\mu} \frac{dE}{|dE/dx|} \frac{1-\beta}{\beta}, \quad (16)$$

where  $E_\mu$  is the MCP energy when it enters the muon counter, and the MCP velocity is  $\beta \equiv \sqrt{1 - m_\chi^2/E^2}$ . Then, the MCP has a time slot of

$$\Delta\tau_\chi \equiv \Delta t_{coll} - \Delta t_{off} - \Delta\tau_\mu$$

to reach the detector while the time window for the data collection is still open. Therefore the MCP must cover the distance  $L - S = L_\mu - S_\mu = 27.5$  m in a shorter time. This travelling through the sandstone is also accompanied with additional time delay due to scattering. This energy loss makes MCP less relativistic. Taking this into account we obtain the following condition for MCP to arrive in time and be recorded,

$$\int_{L_\mu}^L \frac{dx}{\beta c} = \int_{E_L}^{E_\mu} \frac{dE}{|dE/dx|} \frac{1}{\beta} < \Delta\tau_\chi, \quad (17)$$

where  $E_L$  is the MCP energy in the detector.

If the energy losses are small, the energies of MCP in front of the scintillating counters are:  $E_L \approx E - \left| \frac{dE}{dx} \right| L$ ,  $E_\mu \approx E - \left| \frac{dE}{dx} \right| L_\mu$ , if not, it is necessary to solve the equation:

$$\int_{E_L}^{E_i} \frac{dE}{|dE/dx|} = L,$$

where  $dE/dx$  is from Eq.(14) and takes into account the energy loss in matter. To solve this equation we adopt the approximate expressions from Appendix B.

The second benchmark condition is associated with the detector angular acceptance of 2 mr. We estimate the multiple scattering angle of MCP as a function of energy it has in front of the detector ( $E_L$ ) by using Eq. (9, 11) and require it to be:

$$\theta_\chi = \sqrt{\theta_Z^2 + \theta_e^2} < 2 \text{ mr}. \quad (18)$$

### C. Revised exclusion plot

We have explained previously, all the steps towards reevaluation of the SLACmQ bounds on models with MCP. All the numerical calculation we perform with the approximate spectrum of MCP presented in Ref. [54]. In Fig. 6 we show the resulted exclusion region in  $(m_\chi, \epsilon_\chi)$

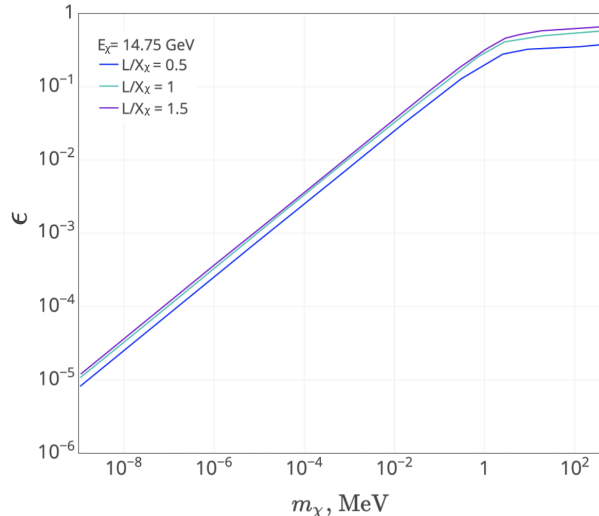
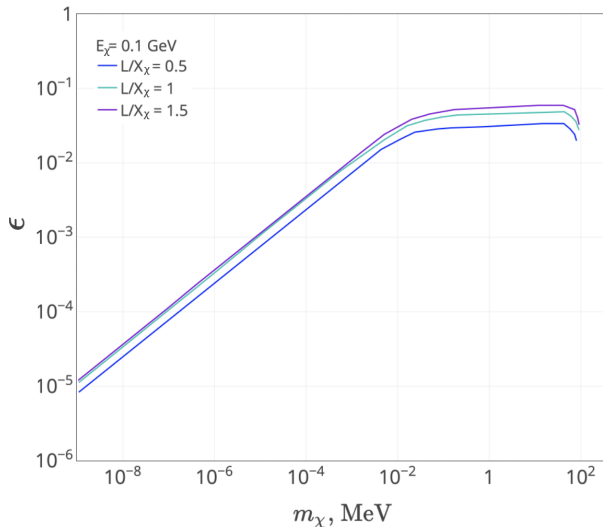


FIG. 5. Illustration of the stopping power for two examples of MCP initial energies.

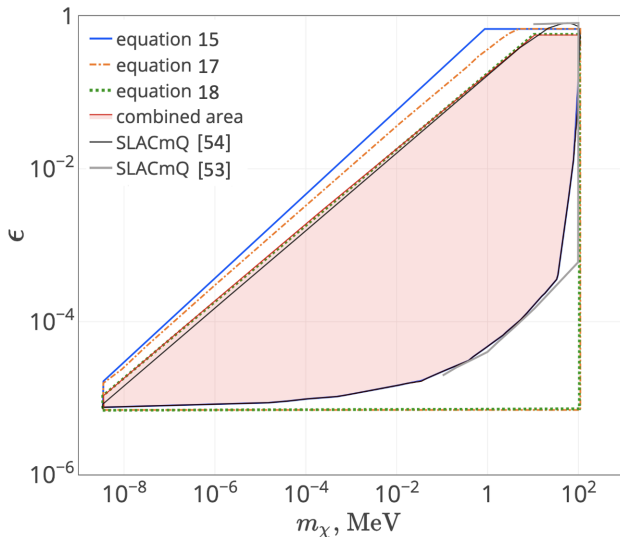


FIG. 6. Regions bounded from Eqs. (15, 17, 18) and the combined exclusion region from our analysis of the SLACmQ data. The obtained region closely matches the result of Ref. [54] (solid black line) and refines that published in the original SLACmQ paper [53] (solid grey line).

plane which is determined by Eqs. (15), (17), (18). Expectedly, the MCP scatterings are mostly important for relatively large charges and small masses. Most critical are deflections of the MCP trajectories depicted by the green dashed line.

The obtained in this way region is similar to the one presented in Ref. [54]. As one can see from Fig. 6, the exclusion region from the original publication [53] of the SLACmQ collaboration is rather limited in mass and has no upper bounds. What is more important, there is a triangular region at  $\epsilon \sim 10^{-3}$  and  $m_\chi \sim 100$  MeV, which we

find not constrained from the SLACmQ data, contrary to their publication. This region is also open in Ref. [54]. It is worth mentioning again that we adopt the lower edge of the curve SLACmQ [54] shown in Fig. 6 from Fig. 5.17 of the Ref. [54]. The numerical values of the regarding coupling correspond to the  $\epsilon$  in Eq. (15).

#### IV. CALCULATION OF THE DOUBLE-DIFFERENTIAL CROSS SECTION OF MCP PAIR PRODUCTION

In this Section we describe our procedure of calculation the double-differential cross section of MCP production in electron scattering off nucleus. At the sufficiently small MCP charge the production happens mostly through emission of the virtual photon,

$$e(p_1)N(\mathcal{P}_2) \rightarrow e(p_3)\gamma^*(p_{\chi_1} + p_{\chi_2})N(\mathcal{P}_4) \rightarrow \quad (19) \\ \rightarrow e(p_3)\chi(p_{\chi_1})\bar{\chi}(p_{\chi_2})N(\mathcal{P}_4),$$

and since it is purely electromagnetic process we calculate it in the exact tree-level approach. The Feynman diagrams referring to the tree-level amplitude are presented in Fig. 7. This contribution is linear in  $\epsilon$ , and we neglect contributions proportional to  $\epsilon^2$  coming from other diagrams.

The NA64e experiment utilizes the electron beam of  $E_1 = 100$  GeV and lead target (see below Sec. V). We carry out the integration of squared exact tree-level amplitude over the phase space of the process (19) by exploiting the latest version of the `CalcHEP` package [57]. The vertex for  $NN\gamma$  interaction we take to be

$$ieZF(-q^2)\gamma_\mu. \quad (20)$$

It corresponds to the spin-1/2 nucleus interaction with photon, here  $q = (\mathcal{P}_2 - \mathcal{P}_4)$  is nucleus transfer momen-

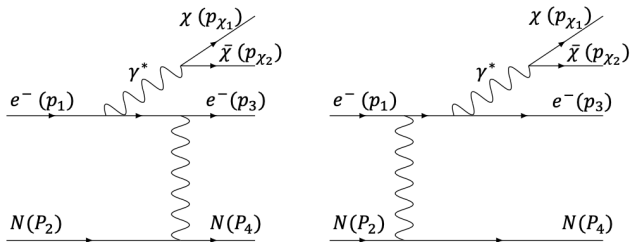


FIG. 7. Leading Feynman diagrams for MCP pair production process.

tum,  $\mathcal{P}_2$  and  $\mathcal{P}_4$  are initial and final momenta of the nucleus. The elastic form-factor  $F(-q^2)$  has the following form

$$F(t) = \frac{a^2 t}{(1 + a^2 t)} \frac{1}{(1 + t/d)}, \quad (21)$$

where  $t = -q^2$  is the squared transfer momentum,  $a = 111Z^{-1/3}/m_e$  and  $d = 0.164A^{-2/3} \text{ GeV}^2$  are screening and nucleus parameters respectively. For the lead active target (atomic number  $A = 207$ , nuclear charge  $Z = 82$ ) of NA64e one estimates the following typical momenta transfer associated with screening effects and nucleus size respectively:  $\sqrt{t_a} = 1/a \simeq 2 \cdot 10^{-5} \text{ GeV}$  and  $\sqrt{t_d} = \sqrt{d} \simeq 6.7 \cdot 10^{-2} \text{ GeV}$ .

We implement the form factor (20), (21) in the C++ code of CalCHEP and carry out VEGAS Monte-Carlo integration of the cross section for various masses  $m_\chi$  in order to obtain the differential energy spectra of the produced MCP. Before presenting its form let us note, that to check our calculations we integrate the double-differential cross section over the MCP energies and thus evaluate the total MCP production cross section which is shown in Fig. 8 as a function of MCP mass  $m_\chi$ . Similar plot can be found in Fig. 3 of Ref. [58], where the calculation is done in the limit of massless electron and for  $m_\chi > 1 \text{ MeV}$ . We have checked that in this limit our estimate of the total cross section matches with that of Ref. [58] with accuracy of a few percent.<sup>1</sup> Therefore, in our study we extend the previous work on (much) lighter MCP and account corrections due to non-zero electron mass.

## V. SENSITIVITY OF NA64e

Before evaluating the MCP search sensitivity with the NA64e experiment, let us briefly describe its main features relevant for further discussion. The NA64e detector is schematically shown in Fig. 9. The experiment employed the optimized H4 100 GeV electron beam

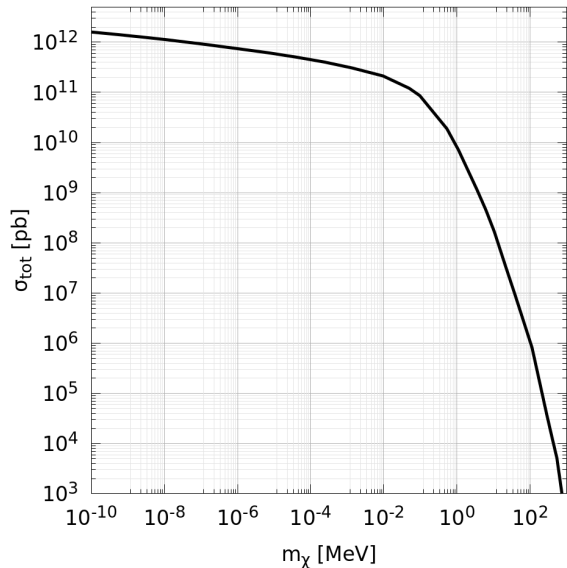


FIG. 8. Total cross section of MCP pair production as the function of  $m_\chi$  for  $E_{beam} = 100 \text{ GeV}$  and  $\epsilon = 1$ .

from the CERN SPS. The beam has a maximal intensity  $\simeq 10^7$  electrons per SPS spill of 4.8 s produced by the primary 400 GeV proton beam with an intensity of few  $10^{12}$  protons on target. The detector utilized the beam defining scintillator (Sc) counters  $S_{1-4}$  and veto  $V_{1,2}$ , a magnetic spectrometer consisting of two successive dipole Magnets<sub>1,2</sub> with the integral magnetic field of  $\simeq 7 \text{ T}\cdot\text{m}$  and a low-material-budget tracker. The tracker was a set of two upstream Micromegas chambers  $T_{1,2}$ , and two downstream MM<sub>3,4</sub>, allowing the measurements of  $e^-$  momenta with the precision  $\delta p/p \simeq 1\%$ . To significantly improve the electron identification, the synchrotron radiation (SR) emitted in the magnetic field of the Magnets<sub>1,2</sub> was used for their tagging with a SR detector (SRD) [59, 60]. By using this method the initial fraction of the hadrons in the beam  $\pi/e^- \lesssim 10^{-2}$  was further suppressed by a factor  $\simeq 10^3$ . The detector was also equipped with an active target, which is an electromagnetic calorimeter (ECAL), a matrix of  $6 \times 6$  Shashlik-type counters assembled from lead and scintillator plates for measurement of the electron energy  $E_{ECAL}$ . Each counter has  $\simeq 40$  radiation lengths ( $X_0$ ) with the first  $4X_0$  serving as a preshower detector. Downstream of the ECAL, the detector was equipped with a large high-efficiency veto counter VETO, and a massive, hermetic hadronic calorimeter (HCAL) of  $\simeq 30$  nuclear interaction lengths in total. The modules HCAL<sub>1-3</sub> provided an efficient veto to detect muons or hadronic secondaries produced in the  $e^-A$  interactions in the target. The search described in this paper uses the data sample of  $N_{EOT} = 2.84 \times 10^{11}$  EOT collected in the three years 2016, 2017 and 2018. The method, briefly discussed in Sec. I and proposed in Refs. [59], is based

<sup>1</sup> We thank J. Pradler, X. Chu and A. Pukhov for helping us to do this cross-check.



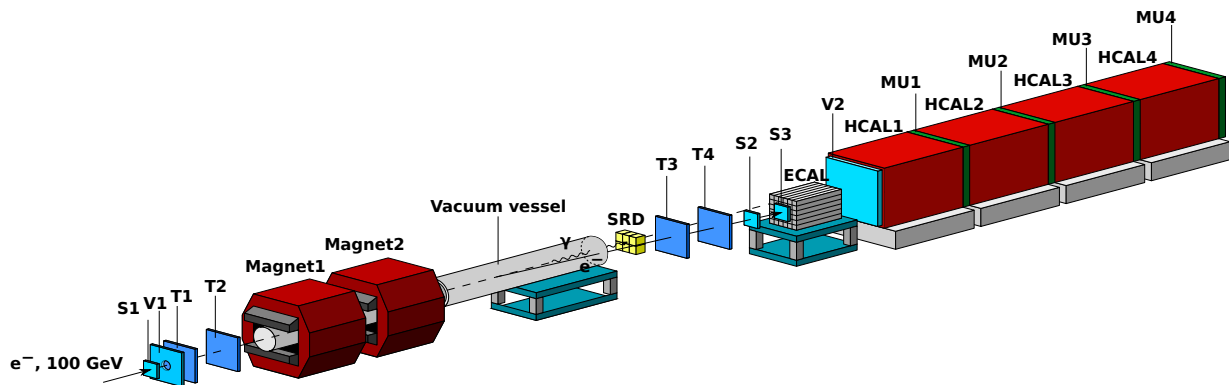


FIG. 9. Schematic illustration of the setup to search for MCP production in the reaction  $e^-N \rightarrow e^-N\gamma^*(\rightarrow \bar{\chi}\chi)$  of 100 GeV  $e^-$  incident on the active ECAL target. See text.

on the detection of the missing energy, carried away by the hard bremsstrahlung MCPs produced in the process  $e^-N \rightarrow e^-N\gamma^*(\rightarrow \bar{\chi}\chi)$  of high-energy electrons scattering in the active ECAL target. The advantage of NA64 idea compared to the beam dump one is that its sensitivity is proportional to  $\epsilon^2$ . The latter is associated with the  $\chi$  production and its subsequent prompt escaping the detector without interactions in the HCAL modules.

In the following, similar to Ref. [58], we first calculate the number of missing energy events associated with MCP emission by energetic electrons incident on the thin target. The latter implies a single scattering on average and then a rapid degrade of the electron energy due to bremsstrahlung. For the case of NA64e, we assume that the incident electron produces MCP in the first scattering within the first radiation length of the ECAL target of NA64e,  $X_0 \simeq 0.56$  cm. This assumption is justified by the fact that the high energy electron loses most its energy in a single process transferring it to the emitted photon.

Now let us evaluate the sensitivity of NA64e to model parameters of MCP taking into account the energy loss of the millicharged particles in the detector. This energy transfers to the electromagnetic channel which NA64e closely monitors and hence sums with all other sources of electromagnetic activity. The experimental signature of the MCP detection, would be an event with the missing energy  $E_{miss} \gtrsim 50$  GeV, see, e.g. Ref.[61]. The events with lower missing energy are not considered as potentially signal events. Therefore, the estimate of MCP energy loss within the detector is an important step towards understanding prospects of NA64e in testing models with MCP.

The total number of MCP pairs produced in the process  $eN \rightarrow eN\chi\bar{\chi}$  can be calculated as follows

$$N_{\chi\bar{\chi}} = \frac{\rho N_A}{M_A} N_{EOT} X_0 \int_{\text{s.b.}} dE_{\chi_1} dE_{\chi_2} \frac{d\sigma(E_{beam})}{dE_{\chi_1} dE_{\chi_2}}. \quad (22)$$

Here  $N_{EOT}$  is a number of electrons accumulated on target,  $\rho = 11.34$  g cm $^{-3}$  is a density of the lead

ECAL active target,  $M_A = 207$  g mol $^{-1}$  is the atomic mass of the target,  $N_A$  is Avogadro's number,  $E_{beam} = 100$  GeV is the energy of initial electron from the beam, the double-differential cross section of  $\chi\bar{\chi}$  production  $d\sigma/(dE_{\chi_1} dE_{\chi_2})$  is calculated by using CalcHEP as described in Sec.IV. The diplots corresponding to several choices of MCP mass are presented in Fig. 10. Naturally, the distribution is symmetric with respect to interchange of the positive and negative MCP.

The integration over  $E_{\chi_1}$  and  $E_{\chi_2}$  in (22) is performed inside the signal box (s. b.). This region is determined by the missing energy cut of the electromagnetic calorimeter (ECAL) exploited in NA64e,  $E_{miss}^{th} \equiv 50$  GeV, and the initial energy of the electron beam  $E_{beam} = 100$  GeV as follows,

$$E_{miss}^{th} \lesssim E_{\chi_1} + E_{\chi_2} - \Delta E_{\chi_1} - \Delta E_{\chi_2} \lesssim E_{beam}. \quad (23)$$

Here  $E_{\chi_1}$  and  $E_{\chi_2}$  are the MCP energies at production,  $\Delta E_{\chi_1}$  and  $\Delta E_{\chi_2}$  are the total energy depositions of the millicharged particles in the ECAL due to possible electromagnetic rescattering on their way out. These quantities are estimated through the differential energy loss as follows

$$\Delta E_{\chi_{1,2}} = - \int_0^{L_T} \frac{dE_{\chi_{1,2}}}{dx} dx = E_{\chi_{1,2}}(0) - E_{\chi_{1,2}}(L_T) \geq 0,$$

and the integral goes over the effective width of the lead material in ECAL,  $L_T = 22.5$  cm. The MCP energies at the exit from ECAL  $E_{\chi_{1,2}}(L_T)$  can be expressed through the energy of MCP at production  $E_{\chi_{1,2}}(0) = E_{\chi_{1,2}}$  by solving the equation

$$\int_{E_{\chi_{1,2}}(0)}^{E_{\chi_{1,2}}(L_T)} dE_{\chi_{1,2}} \frac{1}{(dE_{\chi_{1,2}}/dx)} = -L_T, \quad (24)$$

where for  $(dE_{\chi_{1,2}}/dx)$  we use numerical approximations collected in Appendix A. Finally, for the given energies of

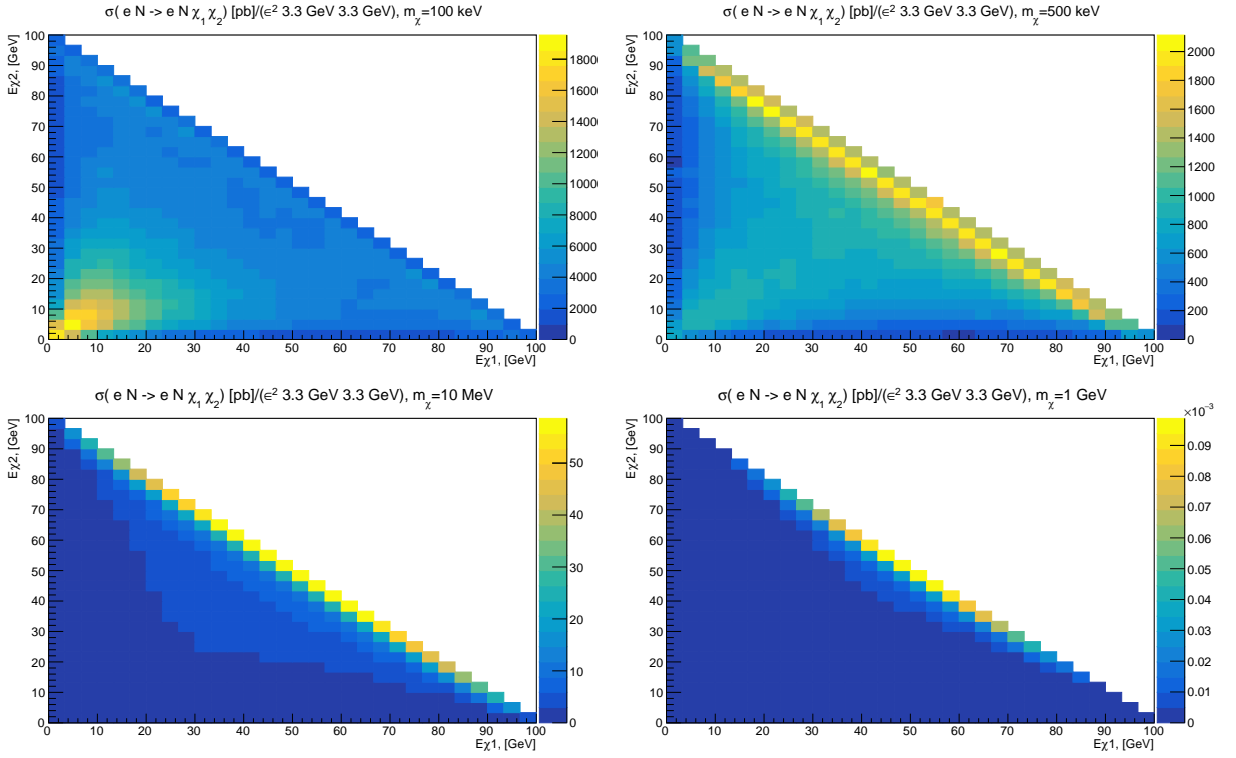


FIG. 10. Double-differential cross section of the MCP pair production as a function of MCP energies  $E_{\chi_1}$  and  $E_{\chi_2}$  for a set of MCP masses  $m_\chi$  and energy of incident electron  $E_{beam} = 100$  GeV. Note that only events above the line  $E_{\chi_1} + E_{\chi_2} > 50$  GeV are interesting with cuts adopted in NA64e experiment.

MCP at production in the target,  $E_{\chi_{1,2}}(0)$ , one has the following region for the signal box

$$E_{miss}^{th} \lesssim E_{\chi_1}(L_T) + E_{\chi_2}(L_T) \lesssim E_{beam}. \quad (25)$$

The relevance of the energy transfer to the electromagnetic cascade is demonstrated in Fig. 11. There we chose three examples of MCP pairs with total energy exceeding the threshold value in NA64e. In the regions above the corresponding lines the MCP lose its energies emitting energetic photons, which are collected by the NA64e ECAL. Finally the total MCP energy drops below the threshold, and so they do not contribute to the signal events.

Numerical calculations reveal that for the wide ranges of  $\epsilon \lesssim 0.3$  and  $m_\chi \lesssim 1$  MeV the radiation energy loss of the millicharged particle (bremsstrahlung) dominates over the energy loss due to ionization,  $\chi e \rightarrow \chi e$ , and due to pair production,  $\chi N \rightarrow \chi N e^+ e^-$ . The energy loss of the millicharged particle due to the bremsstrahlung,  $\chi N \rightarrow \chi N \gamma$ , inside the Pb-target can be approximated for the interesting energetic MCP as follows (see Appendix B)

$$\begin{aligned} \frac{1}{E_\chi} \frac{dE_\chi}{dx} &\simeq -(X_0)^{-1} \epsilon^4 \left( \frac{m_\chi}{m_e} \right)^{-2} \\ &\simeq -0.45 \text{ cm}^{-1} \epsilon^4 \left( \frac{m_\chi}{1 \text{ MeV}} \right)^{-2}. \end{aligned} \quad (26)$$

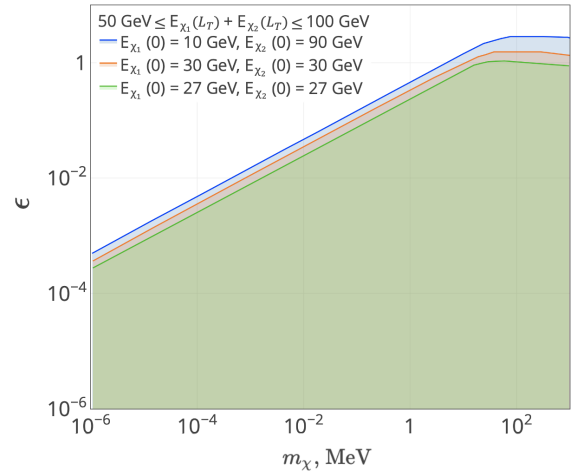


FIG. 11. The MCP pairs with a chosen initial energies do not contribute to the signal events for parameters above the corresponding lines.

It helps to solve (24) for this region of the model parameter space. We note that for  $\epsilon = 1$  and  $m_\chi = m_e$  the result for the electron radiation length  $X_0 \simeq 0.56$  cm is restored from Eq. (26). It implies the well known result that the electron energy is reduced by factor of  $e \simeq 2.71$  within the first radiation length in lead due to the radi-

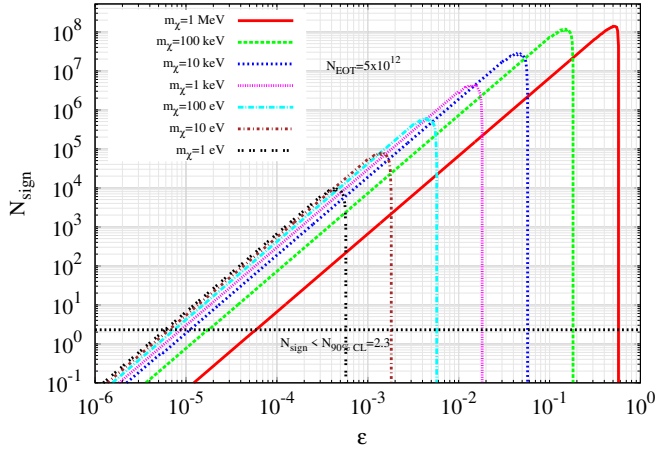


FIG. 12. Number of signal events  $eN \rightarrow eN\gamma^*(\rightarrow \chi\bar{\chi})$  as function of  $\epsilon$ .

ation loss.

Estimated in this way numbers of the signal events are outlined in Fig. 12 for a set of MCP masses and for the projected statistics of  $N_{EOT} = 5 \times 10^{12}$ .

We evaluate the lower 90% C.L. bound on the coupling  $\epsilon$  by requiring  $N_{\chi\bar{\chi}} > s_{up} \equiv 2.3$ , which in the Poisson Statistics corresponds to the null result at zero background (that is a realistic assumption for NA64e and moderate number of incident electrons we utilize). The results are shown in Fig. 13 for the currently accumu-

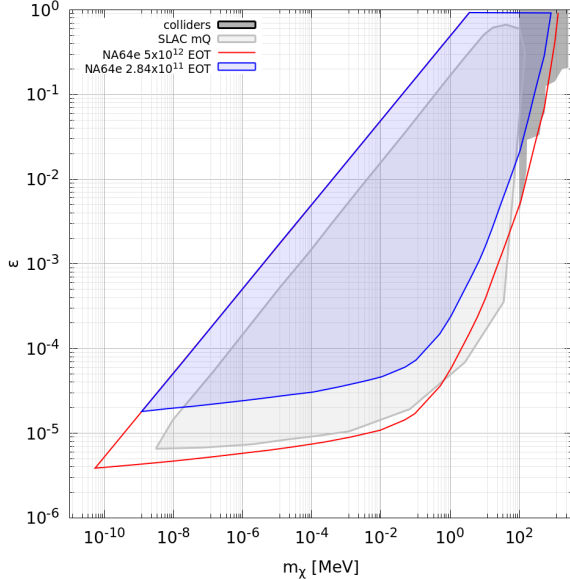


FIG. 13. Sensitivity contours (at 90%CL) of NA64e in the  $(\epsilon, m_\chi)$  plane for the process  $eN \rightarrow eN\gamma^*(\rightarrow \chi\bar{\chi})$ . We account for non-zero electron mass in the calculation,  $m_e \neq 0$ , and suppose that MCP pairs are produced within the first layer (its width is about the electron radiation length) of the lead target. We also set  $\alpha_{QED} = 1/137$ .

lated  $N_{EOT} = 2.84 \times 10^{11}$  and for the projected statistics  $N_{EOT} = 5 \times 10^{12}$  [62].

Concluding this Section we note that it is worth to carry out similar analysis for the MCP sensitivity of the muon fixed target experiments such as NA64 $\mu$  and  $M^3$  (see e. g. Refs. [63–66]). In particular, the signal of muon missing energy events due to the MCP emission can be originated from the following process  $\mu N \rightarrow \mu N\chi\bar{\chi}$ , for which the effects of the MCP passage through the detector should be taken into account. This task is beyond the scope of the present paper and we leave it for future study.

## VI. CONTRIBUTION OF VECTOR MESONS

In this Section we estimate a contribution of vector mesons,  $V = \{\rho, \omega, \phi, J/\psi\}$ , to MCP production at NA64e. We adopt the results of Ref. [67] to estimate the yield of vector mesons produced at NA64e in photonic reaction  $\gamma N \rightarrow NV$  for the expected statistics  $N_{EOT} \simeq 5 \times 10^{12}$ . The invisible branching ratio of mesons to MCP can be written as

$$\text{Br}(V \rightarrow \chi\bar{\chi}) = \epsilon^2 \times \text{Br}(V \rightarrow e^+e^-) \times (1 + 2m_\chi^2/m_V^2) (1 - 4m_\chi^2/m_V^2)^{1/2}. \quad (27)$$

In the absence of signal events, it implies the limit on  $\epsilon$  for each meson mode,  $V \rightarrow \chi\bar{\chi}$ , of the following form

$$\epsilon \gtrsim N_V^{-1/2} \cdot s_{up}^{1/2} \cdot (\text{Br}(V \rightarrow e^+e^-))^{-1/2} \times \quad (28)$$

$$\times (1 + 2m_\chi^2/m_V^2)^{-1/2} (1 - 4m_\chi^2/m_V^2)^{-1/4}. \quad (29)$$

Here  $N_V$  denotes the total number of  $V$ -mesons produced at NA64, which is taken from Tab. II of Ref. [67]. In Fig. 14 we show the corresponding limits in  $(\epsilon, m_\chi)$  plane. One observes a patch around  $m_\chi \simeq 1$  GeV and  $\epsilon \simeq 2 \cdot 10^{-2}$  in the allowed region which can be probed at NA64e with MCP from decays of  $J/\psi$ .

## VII. CONCLUSIONS

In the present paper we investigate various effects associated with MCP passage through the matter. In particular, we discuss in detail the MCP energy losses in matter due to the ionization, bremsstrahlung and  $e^+e^-$  pair production. We also discuss the effects of the MCP trajectory deflection due to the multiple scattering in the matter. We implement these results to revise the bounds on the MCP parameters from SLACmQ experimental data. We find that our results are in a good agreement with the previous study [54]. Our study opens a part of the model parameter space previously considered as excluded on the base of published SLACmQ results [53].

In addition, by exploiting the state-of-the-art CalcHEP package we calculate the exact tree-level cross section

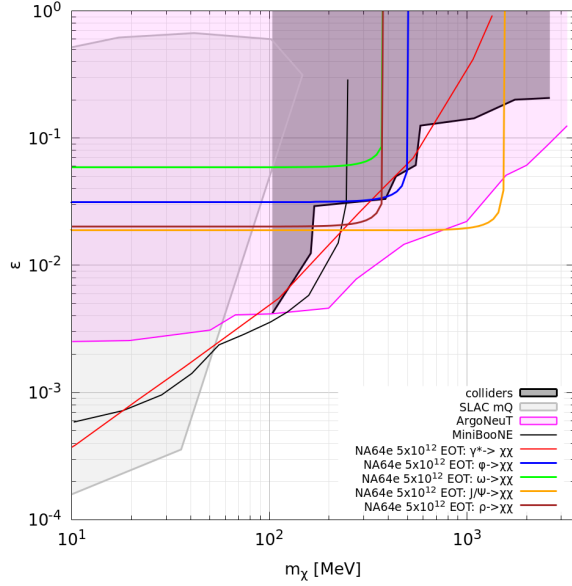


FIG. 14. The expected sensitivity (90% C.L.) of NA64e in the  $(\epsilon, m_\chi)$  plane. We take into account invisible decays of vector mesons to the MCP,  $V \rightarrow \chi\bar{\chi}$ , and MCP production by the energetic beam electrons via bremsstrahlung-like mode  $\gamma^* \rightarrow \chi\bar{\chi}$  for the prospect statistics  $N_{EOT} = 5 \times 10^{12}$  and MCP mass range  $10 \text{ MeV} \leq m_\chi \leq 1.5 \text{ GeV}$ .

of the electron scattering off nucleus  $e^-N \rightarrow e^-N\gamma^*(\rightarrow \chi\bar{\chi})$  to estimate the sensitivity of NA64e fixed target experiment to MCP parameters. We find that the bremsstrahlung reaction  $\chi N \rightarrow \chi N\gamma$  is the dominant process of MCP energy losses in the detector of NA64e for the parameter space of interest  $\epsilon \lesssim 0.1$  and  $m_\chi \lesssim 1 \text{ MeV}$ . To summarise, NA64e can test the models with MCP masses from about  $10^{-4} \text{ eV}$  to  $1 \text{ GeV}$ . In particular, we show that for the expected statistics of electrons incident on target  $N_{EOT} \simeq 5 \times 10^{12}$  at NA64e the relatively light MCP with  $m_\chi \simeq 10^{-4} \text{ eV}$  and  $\epsilon \simeq 10^{-5}$  can be directly probed provided by the bremsstrahlung-like missing energy process  $e^-N \rightarrow e^-N\gamma^*(\rightarrow \chi\bar{\chi})$ , while the relatively large MCP with  $m_\chi \simeq 1 \text{ GeV}$  and  $\epsilon \simeq 2 \cdot 10^{-2}$  can be examined thanks to the invisible vector meson decay signature  $eN \rightarrow eN J/\psi(\rightarrow \chi\bar{\chi})$ .

*Acknowledgements.* We would like to thank R. Capdevilla, A. Celentano, X. Chu, P. Crivelli, S. Demidov, D. Forbes, Y. Kahn, M. Kirsanov, N. Krasnikov, G. Krnjaic, G. Lanfranchi, V. Lyubovitskij, L. Molina Bueno, J. Pradler, A. Prinz, A. Pukhov, G. Rubtsov, P. Satunin, P. Schuster, H. Sieber, F. Tkachov<sup>2</sup> and A. Zhevlakov for very helpful discussions and correspondences. The work on the estimate of the expected sensitivity of NA64e is partly supported by the Russian Science Foundation RSF grant 21-12-00379. The work of

NA on refining SLACmQ sensitivity was supported by the grant of "BASIS" Foundation 21-2-1-100-1.

### Appendix A: Factors for the spectrum of pair production

The function is defined by

$$G = -A g \left( \frac{1}{1+\xi} \right) - B \xi \log \left( 1 + \frac{1}{\xi} \right) - \frac{C}{1+\xi} + \left( 2 \log \frac{E_{e^+} E_{e^-}}{2m_e \omega \sqrt{1+\xi}} - 1 \right) \times \left( A \log \left( 1 + \frac{1}{\xi} \right) + B + \frac{C}{1+\xi} \right) \quad (\text{A1})$$

where

$$A = \left( 1 - \frac{4}{3} \frac{E_{e^+} E_{e^-}}{\omega^2} \right) \left( 1 + \frac{\omega^2}{2E_\chi E'_\chi} \right) + \frac{4}{3} \xi \left( 1 - \frac{E_{e^+} E_{e^-}}{\omega^2} \right),$$

$$B = \frac{4}{3} \frac{E_{e^+} E_{e^-}}{\omega^2} - 1, \quad C = -\frac{\xi}{3} - \frac{1}{6} \frac{\omega^2}{E_\chi E'_\chi} - \frac{1}{3} \frac{(E_{e^+} - E_{e^-})^2}{\omega^2},$$

$$\xi = \frac{m_\chi^2 E_{e^+} E_{e^-}}{4m_e^2 E_\chi (E_\chi - \omega)}, \quad g(x) = -\int_0^x \log \frac{|1-t|}{t} dt,$$

and

$$\omega = E_{e^+} + E_{e^-}, \quad E_\chi = E_{\chi'} + \omega.$$

### Appendix B: Numerical approximation for the energy loss

This Appendix presents the approximation formulae for the MCP energy loss due to bremsstrahlung and  $e^+e^-$  pair production. The bremsstrahlung energy losses can be approximated as:

$$\left| \frac{dE_\chi}{dx} \right|_{\text{brems. approx}} \approx 0.45 \text{ cm}^{-1} E_\chi \epsilon^4 \left( \frac{m_\chi}{1 \text{ MeV}} \right)^{-2}$$

The MCP energy loss due to  $e^+e^-$  pair production can be described by different expressions for different ranges of MCP mass:

$$\left| \frac{dE_\chi}{dx} \right|_{e^+e^- \text{ pair approx}} = \quad (\text{B1})$$

$$10^{-a_i} \epsilon^2 \left( \frac{E_\chi}{1 \text{ MeV}} \right)^{d_i} \left( \frac{m_\chi}{1 \text{ MeV}} \right)^{c_i} [\text{MeV cm}^{-1}] \quad (\text{B2})$$

<sup>2</sup> Deceased

where  $e_{i-1} < \frac{m_\chi}{\text{MeV}} < e_i$ , and  $i = 1, \dots, 5$ , values of the coefficients are shown below:  $e_0 = 0$ ,

$a_1 = 1.9281$	$c_1 = -0.0805$	$d_1 = 1.1340$	$e_1 = 2.154 \times 10^{-4}$
$a_2 = 2.3194$	$c_2 = -0.1964$	$d_2 = 1.1374$	$e_2 = 0.1551$
$a_3 = 2.7185$	$c_3 = -0.5705$	$d_3 = 1.1477$	$e_3 = 4.1596$
$a_4 = 2.6936$	$c_4 = -0.3986$	$d_4 = 1.1138$	$e_4 = 12.4520$
$a_5 = 2.8549$	$c_5 = 0.1423$	$d_5 = 1.0096$	$e_5 = 1 \times 10^3$

Recall Sec. II, that the ionization loss of MCP is negligible for the interesting energetic MCP,  $E_\chi > 10 \text{ GeV}$ . Thus the approximate overall energy loss of high energy MCP is given by the sum

$$\left. \frac{dE_\chi}{dx} \right|_{\text{rad. approx.}} = \left. \frac{dE_\chi}{dx} \right|_{\text{brems. approx.}} + \left. \frac{dE_\chi}{dx} \right|_{e^+e^- \text{ pair approx.}}$$

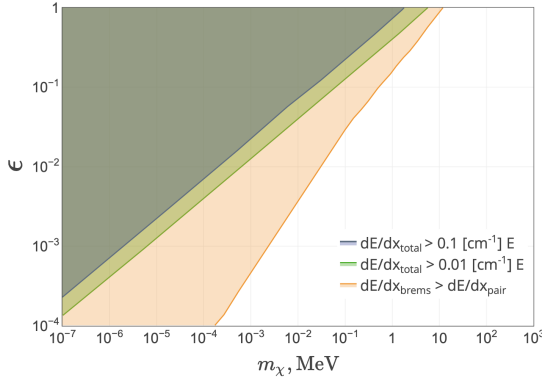


FIG. 15. The bremsstrahlung energy losses dominate in the orange area. In the regions colored dark green, the energy losses can not be considered as small.

- 
- [1] A. Y. Ignatiev, V. A. Kuzmin and M. E. Shaposhnikov, “Is the Electric Charge Conserved?,” *Phys. Lett. B* **84** (1979), 315-318
- [2] D. E. Brahm and L. J. Hall, “U(1)-prime DARK MATTER,” *Phys. Rev. D* **41** (1990), 1067
- [3] M. Pospelov, A. Ritz and M. B. Voloshin, “Secluded WIMP Dark Matter,” *Phys. Lett. B* **662** (2008), 53-61 [arXiv:0711.4866 [hep-ph]].
- [4] J. L. Feng, M. Kaplinghat, H. Tu and H. B. Yu, “Hidden Charged Dark Matter,” *JCAP* **07** (2009), 004 [arXiv:0905.3039 [hep-ph]].
- [5] J. M. Cline, Z. Liu and W. Xue, “Millicharged Atomic Dark Matter,” *Phys. Rev. D* **85** (2012), 101302 [arXiv:1201.4858 [hep-ph]].
- [6] S. Tulin, H. B. Yu and K. M. Zurek, “Resonant Dark Forces and Small Scale Structure,” *Phys. Rev. Lett.* **110** (2013) no.11, 111301 [arXiv:1210.0900 [hep-ph]].
- [7] H. Liu, N. J. Outmezguine, D. Redigolo and T. Volansky, “Reviving Millicharged Dark Matter for 21-cm Cosmology,” *Phys. Rev. D* **100** (2019) no.12, 123011 [arXiv:1908.06986 [hep-ph]].
- [8] C. Creque-Sarbinowski, L. Ji, E. D. Kovetz and M. Kamionkowski, “Direct millicharged dark matter cannot explain the EDGES signal,” *Phys. Rev. D* **100** (2019) no.2, 023528 [arXiv:1903.09154 [astro-ph.CO]].
- [9] R. Harnik, Z. Liu and O. Palamara, “Millicharged Particles in Liquid Argon Neutrino Experiments,” *JHEP* **07** (2019), 170 [arXiv:1902.03246 [hep-ph]].
- [10] B. Holdom, “Two U(1)’s and Epsilon Charge Shifts,” *Phys. Lett. B* **166** (1986), 196-198
- [11] E. Izaguirre and I. Yavin, “New window to millicharged particles at the LHC,” *Phys. Rev. D* **92** (2015) no.3, 035014 [arXiv:1506.04760 [hep-ph]].
- [12] Z. Liu and Y. Zhang, “Probing millicharge at BESIII via monophoton searches,” *Phys. Rev. D* **99** (2019) no.1, 015004 [arXiv:1808.00983 [hep-ph]].
- [13] Y. Zhang, W. T. Zhang, M. Song, X. A. Pan, Z. M. Niu and G. Li, “Probing invisible decay of dark photon at BESIII and future STCF via monophoton searches,” *Phys. Rev. D* **100** (2019) no.11, 115016 [arXiv:1907.07046 [hep-ph]].

- [14] Z. Liu, Y. H. Xu and Y. Zhang, “Probing dark matter particles at CEPC,” *JHEP* **06** (2019), 009 [arXiv:1903.12114 [hep-ph]].
- [15] J. Liang, Z. Liu, Y. Ma and Y. Zhang, “Millicharged particles at electron colliders,” *Phys. Rev. D* **102** (2020) no.1, 015002 [arXiv:1909.06847 [hep-ph]].
- [16] Y. Bai, S. J. Lee, M. Son and F. Ye, “Muon g-2 from Millicharged Hidden Confining Sector,” *JHEP* **11** (2021), 019 [arXiv:2106.15626 [hep-ph]].
- [17] A. Ball, G. Beauregard, J. Brooke, C. Campagnari, M. Carrigan, M. Citron, J. De La Haye, A. De Roeck, Y. Elskens and R. E. Franco, *et al.* “Search for millicharged particles in proton-proton collisions at  $\sqrt{s} = 13$  TeV,” *Phys. Rev. D* **102** (2020) no.3, 032002 [arXiv:2005.06518 [hep-ex]].
- [18] A. Ball *et al.* [milliQan], “Sensitivity to millicharged particles in future proton-proton collisions at the LHC with the milliQan detector,” *Phys. Rev. D* **104** (2021) no.3, 032002 [arXiv:2104.07151 [hep-ex]].
- [19] J. Jaeckel, M. Jankowiak and M. Spannowsky, “LHC probes the hidden sector,” *Phys. Dark Univ.* **2** (2013), 111-117 [arXiv:1212.3620 [hep-ph]].
- [20] X. Chu, J. L. Kuo and J. Pradler, “Dark sector-photon interactions in proton-beam experiments,” *Phys. Rev. D* **101** (2020) no.7, 075035 [arXiv:2001.06042 [hep-ph]].
- [21] K. J. Kelly and Y. D. Tsai, “Proton fixed-target scintillation experiment to search for millicharged dark matter,” *Phys. Rev. D* **100** (2019) no.1, 015043 [arXiv:1812.03998 [hep-ph]].
- [22] J. H. Kim, I. S. Hwang and J. H. Yoo, “Search for sub-millicharged particles at J-PARC,” *JHEP* **05** (2021), 031 [arXiv:2102.11493 [hep-ex]].
- [23] D. Gorbunov, I. Krasnov, Y. Kudenko and S. Suvorov, “Double-hit signature of millicharged particles in 3D segmented neutrino detector,” *Phys. Lett. B* **822** (2021), 136641 [arXiv:2103.11814 [hep-ph]].
- [24] G. Marocco and S. Sarkar, “Blast from the past: Constraints on the dark sector from the BEBC WA66 beam dump experiment,” *SciPost Phys.* **10** (2021) no.2, 043 [arXiv:2011.08153 [hep-ph]].
- [25] G. Magill, R. Plestid, M. Pospelov and Y. D. Tsai, “Millicharged particles in neutrino experiments,” *Phys. Rev. Lett.* **122** (2019) no.7, 071801 [arXiv:1806.03310 [hep-ph]].
- [26] R. Acciarri *et al.* [ArgoNeuT], “Improved Limits on Millicharged Particles Using the ArgoNeuT Experiment at Fermilab,” *Phys. Rev. Lett.* **124** (2020) no.13, 131801 [arXiv:1911.07996 [hep-ex]].
- [27] S. Foroughi-Abari, F. Kling and Y. D. Tsai, “Looking forward to millicharged dark sectors at the LHC,” *Phys. Rev. D* **104** (2021) no.3, 035014 [arXiv:2010.07941 [hep-ph]].
- [28] A. Berlin, N. Blinov, G. Krnjaic, P. Schuster and N. Toro, “Dark Matter, Millicharges, Axion and Scalar Particles, Gauge Bosons, and Other New Physics with LDMX,” *Phys. Rev. D* **99** (2019) no.7, 075001 [arXiv:1807.01730 [hep-ph]].
- [29] G. Afek, F. Monteiro, J. Wang, B. Siegel, S. Ghosh and D. C. Moore, “Limits on the abundance of millicharged particles bound to matter,” *Phys. Rev. D* **104** (2021) no.1, 012004 [arXiv:2012.08169 [hep-ex]].
- [30] E. Gabrielli, L. Marzola, E. Milotti and H. Veermäe, “Polarization observables for millicharged particles in photon collisions,” *Phys. Rev. D* **94** (2016) no.9, 095014 [erratum: *Phys. Rev. D* **95** (2017) no.11, 119903] [arXiv:1604.00393 [hep-ph]].
- [31] D. C. Moore, A. D. Rider and G. Gratta, “Search for Millicharged Particles Using Optically Levitated Microspheres,” *Phys. Rev. Lett.* **113** (2014) no.25, 251801 [arXiv:1408.4396 [hep-ex]].
- [32] A. Berlin and A. Hook, “Searching for Millicharged Particles with Superconducting Radio-Frequency Cavities,” *Phys. Rev. D* **102** (2020) no.3, 035010 [arXiv:2001.02679 [hep-ph]].
- [33] R. Harnik, R. Plestid, M. Pospelov and H. Ramani, “Millicharged cosmic rays and low recoil detectors,” *Phys. Rev. D* **103** (2021) no.7, 075029 [arXiv:2010.11190 [hep-ph]].
- [34] A. D. Dolgov and A. S. Rudenko, “Relic abundance of MeV millicharged particles,” *J. Exp. Theor. Phys.* **124** (2017) no.4, 564-569 [arXiv:1609.07773 [hep-ph]].
- [35] J. T. Li and T. Lin, “Dynamics of millicharged dark matter in supernova remnants,” *Phys. Rev. D* **101** (2020) no.10, 103034 [arXiv:2002.04625 [astro-ph.CO]].
- [36] A. Aboubrahim, P. Nath and Z. Y. Wang, “A cosmologically consistent millicharged dark matter solution to the EDGES anomaly of possible string theory origin,” *JHEP* **12** (2021), 148 [arXiv:2108.05819 [hep-ph]].
- [37] S. Davidson, S. Hannestad and G. Raffelt, “Updated bounds on millicharged particles,” *JHEP* **05** (2000), 003 [arXiv:hep-ph/0001179 [hep-ph]].
- [38] H. Vogel and J. Redondo, “Dark Radiation constraints on minicharged particles in models with a hidden photon,” *JCAP* **02** (2014), 029 [arXiv:1311.2600 [hep-ph]].
- [39] A. Caputo, L. Sberna, M. Frias, D. Blas, P. Pani, L. Shao and W. Yan, “Constraints on millicharged dark matter and axionlike particles from timing of radio waves,” *Phys. Rev. D* **100** (2019) no.6, 063515 [arXiv:1902.02695 [astro-ph.CO]].
- [40] M. Korwar and A. M. Thalappilil, “Novel Astrophysical Probes of Light Millicharged Fermions through Schwinger Pair Production,” *JHEP* **04** (2019), 039 [arXiv:1709.07888 [hep-ph]].
- [41] D. Ejlli, “Millicharged fermion vacuum polarization in a cosmic magnetic field and generation of CMB elliptic polarization,” *Phys. Rev. D* **96** (2017) no.2, 023540 [arXiv:1704.01894 [hep-ph]].
- [42] X. Huang, X. P. Zheng, W. H. Wang and S. Z. Li, “Constraints on millicharged particles by neutron stars,” *Phys. Rev. D* **91** (2015) no.12, 123513 [arXiv:1509.07620 [astro-ph.HE]].
- [43] A. D. Dolgov, S. L. Dubovsky, G. I. Rubtsov and I. I. Tkachev, “Constraints on millicharged particles from Planck data,” *Phys. Rev. D* **88** (2013) no.11, 117701 [arXiv:1310.2376 [hep-ph]].
- [44] A. Melchiorri, A. Polosa and A. Strumia, “New bounds on millicharged particles from cosmology,” *Phys. Lett. B* **650** (2007), 416-420 [arXiv:hep-ph/0703144 [hep-ph]].
- [45] S. L. Dubovsky, D. S. Gorbunov and G. I. Rubtsov, “Narrowing the window for millicharged particles by CMB anisotropy,” *JETP Lett.* **79** (2004), 1-5 [arXiv:hep-ph/0311189 [hep-ph]].
- [46] C. A. Argüelles Delgado, K. J. Kelly and V. Muñoz Albornoz, “Millicharged particles from the heavens: single- and multiple-scattering signatures,” *JHEP* **11** (2021), 099 [arXiv:2104.13924 [hep-ph]].
- [47] M. Kachelriess and J. Tjemsland, “Meson production in air showers and the search for light exotic particles,”

- Astropart. Phys. **132** (2021), 102622 [arXiv:2104.06811 [hep-ph]].
- [48] R. Plestid, V. Takhistov, Y. D. Tsai, T. Bringmann, A. Kusenko and M. Pospelov, “New Constraints on Millicharged Particles from Cosmic-ray Production,” Phys. Rev. D **102** (2020), 115032 [arXiv:2002.11732 [hep-ph]].
- [49] L. Singh *et al.* [TEXONO], “Constraints on millicharged particles with low threshold germanium detectors at Kuo-Sheng Reactor Neutrino Laboratory,” Phys. Rev. D **99** (2019) no.3, 032009 [arXiv:1808.02719 [hep-ph]].
- [50] J. W. Chen, H. C. Chi, H. B. Li, C. P. Liu, L. Singh, H. T. Wong, C. L. Wu and C. P. Wu, “Constraints on millicharged neutrinos via analysis of data from atomic ionizations with germanium detectors at sub-keV sensitivities,” Phys. Rev. D **90** (2014) no.1, 011301 [arXiv:1405.7168 [hep-ph]].
- [51] S. N. Gninenko, N. V. Krasnikov and A. Rubbia, “Search for millicharged particles in reactor neutrino experiments: A Probe of the PVLAS anomaly,” Phys. Rev. D **75** (2007), 075014 [arXiv:hep-ph/0612203 [hep-ph]].
- [52] S. N. Gninenko, D. V. Kirpichnikov and N. V. Krasnikov, “Probing millicharged particles with NA64 experiment at CERN,” Phys. Rev. D **100** (2019) no.3, 035003 [arXiv:1810.06856 [hep-ph]].
- [53] A. A. Prinz, R. Baggs, J. Ballam, S. Ecklund, C. Fertig, J. A. Jaros, K. Kase, A. Kulikov, W. G. J. Langeveld and R. Leonard, *et al.* “Search for millicharged particles at SLAC,” Phys. Rev. Lett. **81** (1998), 1175-1178 [arXiv:hep-ex/9804008 [hep-ex]].
- [54] A. A. Prinz, “The Search for millicharged particles at SLAC,” SLAC-R-569.
- [55] P. A. Zyla *et al.* [Particle Data Group], “Review of Particle Physics,” PTEP **2020** (2020) no.8, 083C01
- [56] V. N. Bayer, V. M. Katkov, V. S. Fadin, Radiation of relativistic electrons, Atomizdat, Moscow (1973).
- [57] A. Belyaev, N. D. Christensen and A. Pukhov, “CalcHEP 3.4 for collider physics within and beyond the Standard Model,” Comput. Phys. Commun. **184** (2013), 1729-1769 [arXiv:1207.6082 [hep-ph]].
- [58] X. Chu, J. Pradler and L. Semmelrock, “Light dark states with electromagnetic form factors,” Phys. Rev. D **99** (2019) no.1, 015040 [arXiv:1811.04095 [hep-ph]].
- [59] S. N. Gninenko, “Search for MeV dark photons in a light-shining-through-walls experiment at CERN,” Phys. Rev. D **89** (2014) no.7, 075008 [arXiv:1308.6521 [hep-ph]].
- [60] E. Depero, D. Banerjee, V. Burtsev, A. Chumakov, D. Cooke, A. V. Dermenev, S. V. Donskov, F. Dubinin, R. R. Dusaev and S. Emmenegger, *et al.* “High purity 100 GeV electron identification with synchrotron radiation,” Nucl. Instrum. Meth. A **866** (2017), 196-201 [arXiv:1703.05993 [physics.ins-det]].
- [61] D. Banerjee, V. E. Burtsev, A. G. Chumakov, D. Cooke, P. Crivelli, E. Depero, A. V. Dermenev, S. V. Donskov, R. R. Dusaev and T. Enik, *et al.* “Dark matter search in missing energy events with NA64,” Phys. Rev. Lett. **123** (2019) no.12, 121801 [arXiv:1906.00176 [hep-ex]].
- [62] D. Banerjee *et al.* [NA64], “Search for invisible decays of sub-GeV dark photons in missing-energy events at the CERN SPS,” Phys. Rev. Lett. **118** (2017) no.1, 011802 [arXiv:1610.02988 [hep-ex]].
- [63] H. Sieber, D. Banerjee, P. Crivelli, E. Depero, S. N. Gninenko, D. V. Kirpichnikov, M. M. Kirsanov, V. Poliakov and L. Molina Bueno, “Prospects in the search for a new light  $Z'$  boson with the NA64 $\mu$  experiment at the CERN SPS,” [arXiv:2110.15111 [hep-ex]].
- [64] D. V. Kirpichnikov, H. Sieber, L. M. Bueno, P. Crivelli and M. M. Kirsanov, “Probing hidden sectors with a muon beam: Total and differential cross sections for vector boson production in muon bremsstrahlung,” Phys. Rev. D **104** (2021) no.7, 076012 [arXiv:2107.13297 [hep-ph]].
- [65] Y. Kahn, G. Krnjaic, N. Tran and A. Whitbeck, “ $M^3$ : a new muon missing momentum experiment to probe  $(g - 2)_\mu$  and dark matter at Fermilab,” JHEP **09** (2018), 153 [arXiv:1804.03144 [hep-ph]].
- [66] R. Capdevilla, D. Curtin, Y. Kahn and G. Krnjaic, “Systematically Testing Singlet Models for  $(g - 2)_\mu$ ,” [arXiv:2112.08377 [hep-ph]].
- [67] P. Schuster, N. Toro and K. Zhou, “Probing invisible vector meson decays with the NA64 and LDMX experiments,” Phys. Rev. D **105** (2022) no.3, 035036 [arXiv:2112.02104 [hep-ph]].